Oil in water injection from a submerged nozzle

C. Georgescu, Edouard Canot, Jean-Luc Achard

OIL IN WATER INJECTION FROM A SUBMERGED NOZZLE

Sanda-Carmen GEORGESCU, Assoc. Prof.*
Hydraulics Department
University "Politehnica" of Bucharest

Édouard CANOT, CNRS Researcher
Laboratory IRISA
INRIA, Rennes, France

Jean-Luc ACHARD, CNRS Research Director
Laboratoire des Écoulements Géophysiques et Industriels
Grenoble, France

**Corresponding author*: 313 Spl. Independentei, S6, 060032, Bucharest, Romania
Tel.: (+40) 21 402 9705, Fax: (+40) 21 402 9865, Email: carmen@hydrop.pub.ro

ABSTRACT

When a certain amount of oil is injected upwardly through a vertical nozzle submerged in water, the oil-water interface evolves, for large orifices, from a sessile shape, to a cap profile with a roll-up border.

The numerical simulation of such liquid-liquid interface evolution was made through the Boundary Element Method (BEM), by assuming a potential flow of a viscous fluid. At the end of the computed process, the velocity field behaviour leads to an inward rolling up movement of the cap border, simultaneously with the interface necking near the orifice level. Such velocity field precedes typically a vortex ring formation.

An olive oil – water couple has been selected, because of the appropriate physical properties of those liquids: comparable densities, huge difference of viscosities, and very small interfacial tension.

KEYWORDS

Vortex ring, interfacial tension, boundary element method

NOMENCLATURE

Fr	[-]	Froude number
R	[m]	orifice radius; length scale
R_1, R_2	[m]	local principal radii of curvature
Re	[-]	Reynolds number
We	[-]	Weber number
dA	[m^2]	axisymmetric surface element
g	[m/s^2]	gravity
n	[m]	normal co-ordinate
p	[Pa]	pressure
r	[m]	radial co-ordinate
s	[m]	curvilinear abscissa
t	[s]	time
$\mathbf{v}$	[m/s]	velocity vector
z	[m]	axial co-ordinate
Δs	[m]	arc length
Δt	[s]	time step
Ω		oil domain in a meridian plane
Σ		surface; oil-water interface
β	[rad]	azimuthal angle
δt_o	[s]	time pulse
ϕ	[m^2/s]	velocity potential
μ	[Pa·s]	dynamic viscosity of the liquid
ρ	[kg/m^3]	density of the liquid
σ	[N/m]	interfacial tension

Subscripts and Superscripts

n	normal direction
o	oil
s	solid wall of the cylindrical nozzle
z	axial direction
w	water
*	dimensionless variable

ABBREVIATIONS

BEM Boundary Element Method

1. INTRODUCTION

A *vortex ring* is produced when the linear momentum is imparted to the fluid with axial symmetry [1]. A familiar example of flow with circular vortex lines is the tobacco *smoke ring*, formed by a particular puffing technique. The upward injection of a small quantity of coloured liquid into a liquid pool [1, plate 20] gives rise to a vortex ring that travels away from the orifice: within the resulted torus, a roll-up movement is developed in cross-section. Similar phenomenon

can be obtained by pushing downward some amount of liquid throughout a submerged nozzle: for such case, the velocity field measured by Particle Image Velocimetry near the viscous vortex ring core has been compared by Dazin *et al*. [2] to theoretical models derived for thin core vortex rings in an inviscid fluid. The velocity field induced by an inviscid vortex ring has been analysed in [3].

It is possible to produce a vortex ring, or toroidal bubble, by injecting a volume of air from a submerged nozzle [1]. The toroidal bubble rebound in collapsing bubble with jet formation and impact [4], as well as the toroidal bubble entrapped within the liquid during a bursting bubble collapse at a free surface [5], or during a plunge of a vertical liquid jet on the free surface of a pool [6], are also associated to vortex rings.

Drops falling into a liquid pool produce vortex rings that penetrate more deeply into the pool [1, 7]. The jet impinging on a cylindrical surface [8], or on a convex surface [9] equally leads to vortex rings formation.

Some complex phenomena also involve vortex ring formation: it is the case of the fuel injection process that can be accompanied by the development of a fountain structure consisting of a spray jet and a vortex ring [10], or the case of unsteady shear flow induced by vortex ring / wall interactions [11].

When a certain amount of oil is injected upwardly through a large nozzle orifice submerged in water, the oil-water interface evolves from a sessile shape, to a cap profile with a roll-up border (Figure 1). At the end of the process, the velocity field behaviour leads to an inward rolling up movement of the cap border, simultaneously with the interface necking near the orifice level. It is expected that after the complete necking and the detachment of the oil drop from the nozzle, the drop interface will break up from a cap shape into a toroidal shape, the torus being formed from the previous cap border roll-up. Such toroidal oil drop corresponds to a *vortex ring* structure, and can be added to the previous examples.

Within the present paper, the numerical simulation of the interface evolution for oil in water injection was made through the Boundary Element Method (BEM), by assuming a potential flow of a viscous fluid [12]. Our computations are not performed till the toroidal oil drop formation, because of the complex phenomenon related to the interface rupture and strong changes of the geometrical configuration. But it is highlighted that when injecting oil in water from a submerged nozzle, for large orifice sizes, the liquid-liquid interface rolls up and creates the velocity field that can lead to a vortex ring formation. It is showed that the phenomenon is strongly dependent on the capillary forces, on the viscous forces (introduced here only through the normal stress at the interface), and on the gravity, the last one being important especially when increasing the nozzle orifice radius. Within the present study, an olive oil – water couple has been selected, because of the appropriate physical properties of those liquids, namely comparable densities, huge difference of viscosities, and very small interfacial tension.

2. PROBLEM STATEMENT

The free boundary problem is axisymmetric. In a meridian plane *r*Oz, the oil domain Ω (Figure 1) is bounded by three surfaces: the oil surface Σ_o in cross-section inside the cylindrical nozzle, the vertical solid wall Σ_s of the nozzle, and the oil-water interface Σ. The unit normal **n** on the boundary points inwards the oil domain. The azimuthal angle β is defined between the radial unit vector and the tangent unit vector **t**.

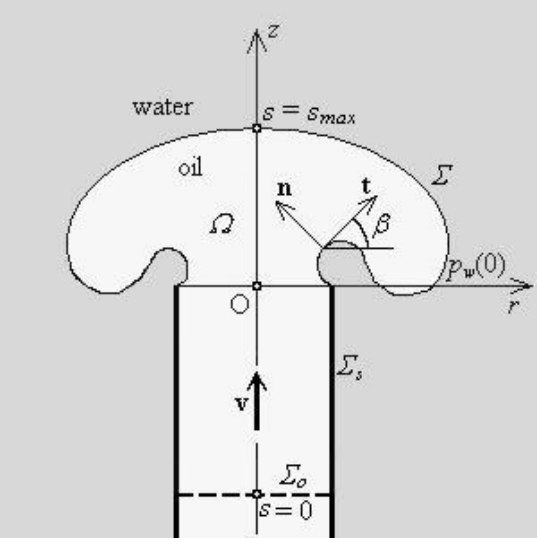

Figure 1. Geometric axisymmetric configuration

The curvilinear abscissa *s* starts from the Oz axis inside the nozzle, follows radially the surface Σ_o, then follows upwards the solid surface Σ_s, then the interface Σ, and reaches its maximum value on the Oz axis, at the apex of the oil-water interface.

The oil flow at the exit of the nozzle is assumed to be potential, with a velocity field $\mathbf{v} = \nabla\phi$. The Laplace equation for the velocity potential ϕ is:

$$\nabla^2\phi = 0 . \qquad (1)$$

The velocity is defined by its normal component $v_n = \partial\phi/\partial n$, and tangential component $\partial\phi/\partial s$.

The Euler's equation for the oil motion is written:

$$\frac{\partial(\nabla\phi)}{\partial t} + \nabla\frac{v^2}{2} = -\frac{1}{\rho_o}\nabla p_o(z) - g\nabla z, \tag{2}$$

where p_o is the oil pressure, and ρ_o the oil density.

The difference between the values of the stress tensor on either side if the oil-water interface is a normal force due wholly to the surface tension [1]. The component of the surface force normal to the interface, namely the normal momentum balance at any point of the interface Σ is written:

$$p_o(z) - 2\mu_o\frac{\partial v_n}{\partial n} - p_w(z) = \sigma\left(\frac{1}{R_1} + \frac{1}{R_2}\right), \tag{3}$$

where μ_o is the oil dynamic viscosity, σ is the oil-water interfacial tension, R_1 and R_2 are the local principal radii of curvature. The water pressure can be defined as: $p_w(z) = p_w(0) - \rho_w g\, z$, where $p_w(0)$ is the hydrostatic pressure at the orifice level, at $z = 0$. Within the balance (3), only the normal viscous stress $2\mu_o(\partial v_n/\partial n)$ on the oil side of the interface has been considered. The normal viscous stress on the water side of the interface has been neglected, due to the water viscosity, which is negligible with respect to the oil viscosity. The oil pressure can be expressed from (3) as:

$$p_o(z) = p_w(0) + \sigma\left(\frac{1}{R_1} + \frac{1}{R_2}\right) - \rho_w g\, z + 2\mu_o\frac{\partial^2\phi}{\partial n^2}. \tag{4}$$

Combining Euler's equation (2) and the normal momentum balance (4) in order to reduce the oil pressure term, we obtain the Bernoulli's equation at any point of the interface Σ:

$$\rho_o\left(\frac{\partial\phi}{\partial t} + \frac{v^2}{2}\right) = -\sigma\left(\frac{1}{R_1} + \frac{1}{R_2}\right) + (\rho_w - \rho_o)g\, z - 2\mu_o\frac{\partial^2\phi}{\partial n^2}. \tag{5}$$

So, within this type of potential model, viscous effects can only be partially considered through the boundary condition [12], namely the normal momentum balance (4) at any point of the fluid-fluid interface Σ.

We adopt the nozzle orifice radius R as length scale, σ/R as pressure scale, $\sqrt{\sigma/(R\rho_o)}$ as velocity scale, and the ratio between length and velocity as time scale. According to the choice of scales, the Weber number takes always the unit value $We = 1$. The Froude number is expressed for the studied problem as:

$$Fr = \frac{\sigma}{(\rho_w - \rho_o)gR^2}, \tag{6}$$

while the Reynolds number is:

$$Re = \frac{\sqrt{\sigma R\rho_o}}{\mu_o}. \tag{7}$$

Dimensionless variables will be denoted by an asterisk.

The dimensionless form of the Bernoulli's equation (5),

$$\frac{\partial\phi^*}{\partial t^*} = -\frac{v^{*2}}{2} - \frac{1}{We}\left(\frac{1}{R_1^*} + \frac{1}{R_2^*}\right) + \frac{1}{Fr}z^* - \frac{2}{Re}\frac{\partial^2\phi^*}{\partial n^{*2}}, \tag{8}$$

gives the local time derivative of the velocity potential, $\partial\phi^*/\partial t^*$. The singularities issued in (8) at $r^* = 0$, are removed by taking into account that on the Oz axis, the axisymmetric curvature $1/R_2^* = (\sin\beta)/r^*$ equals the planar curvature $1/R_1^* = \partial\beta/\partial s^*$. The expressions of the dimensionless normal gradient of normal velocity $\partial^2\phi^*/\partial n^{*2}$ on the Oz axis, and outside of it, are written [13, 14]:

$$\frac{\partial^2\phi^*}{\partial n^{*2}} = -2\frac{\partial^2\phi^*}{\partial s^{*2}} + 2\frac{\partial\beta}{\partial s^*}\frac{\partial\phi^*}{\partial n^*}, \text{ at } r^* = 0, \tag{9}$$

and

$$\frac{\partial^2\phi^*}{\partial n^{*2}} = -\frac{\partial^2\phi^*}{\partial s^{*2}} - \frac{\cos\beta}{r^*}\frac{\partial\phi^*}{\partial s^*} + \left(\frac{\partial\beta}{\partial s^*} + \frac{\sin\beta}{r^*}\right)\frac{\partial\phi^*}{\partial n^*}, \quad \text{at } r^* \neq 0. \tag{10}$$

The global mechanical energy balance can be expressed only in surface integrals terms [14]:

$$\frac{\mathrm{d}}{\mathrm{d}t^*}\left(\frac{1}{2}\int_{\Sigma_\Omega}\phi^*\frac{\partial\phi^*}{\partial n^*}\mathrm{d}A^*+\frac{1}{We}\int_{\Sigma}\mathrm{d}A^*\right)+$$

$$+\frac{\mathrm{d}}{\mathrm{d}t^*}\left(\frac{1}{2Fr}\int_{\Sigma}z^{*2}\mathrm{d}A^*\right)= \qquad (11)$$

$$=-\frac{2}{Re}\int_{\Sigma_\Omega}\frac{\partial\phi^*}{\partial n^*}\frac{\partial^2\phi^*}{\partial n^{*2}}\mathrm{d}A^*\ ,$$

where $\Sigma_\Omega=\Sigma_o\cup\Sigma_s\cup\Sigma$ is the oil domain boundary, and $\mathrm{d}A^*$ the dimensionless axisymmetric surface element. It is highlighted that the right hand term of (11), namely the dissipation of the mechanical energy due to shear viscosity, depends only on the normal component of the velocity, and on the normal second derivative of the velocity potential.

3. NUMERICAL METHOD

The distorted oil-water interface evolution is an axisymmetric transient free-boundary problem that is modelled here through a Boundary Element Method (BEM). An irrotational flow model is appropriate because of the impulsive character of the process. Within the model, viscous effects are partially included through the normal viscous stress at the interface (expressed in terms of the velocity potential), as it is allowed for potential flows of fluids with constant viscosity [12].

The BEM numerical code (built in Fortran), has been successfully used in modelling the highly distorted gas-liquid interface evolution, within a potential flow of a viscous fluid assumption, both for the collapsing bursting bubbles at a free liquid surface, terminated by microjet breaking and droplets ejection [13-16], and for drops formation and ejection from a vertically capillary nozzle, by piezoelectric stimulation [17, 18] (Drop-On-Demand technology).

The transient free-boundary problem is successively divided into tiny time steps Δt^*. There are two types of calculations.

① At a fixed instant t^*, the Laplace equation (1) is solved through BEM, to obtain the velocity potential values $\phi^*(t^*)$, and the corresponding normal component, and tangential component of the velocity. Kinetic conditions of Neumann type are defined on the solid surface Σ_s, where the normal velocity vanishes $v_n^*=\partial\phi^*/\partial n^*=0$. Neumann type conditions are also defined on the oil surface Σ_o inside the nozzle, where the normal velocity has an imposed constant value: $v_n^*(t^*)=v_{no}^*$. During a time pulse δt_o^* at the beginning of the computation, that is for $0\le t^*\le\delta t_o^*$, the normal velocity is $v_{no}^*\neq 0$ (that condition corresponds to the injection of a fixed small amount of oil in water, during a δt_o^* time period). Then, for any moment $t^*>\delta t_o^*$, the normal velocity vanishes: $v_{no}^*=0$ (meaning that the oil injection is stopped for $t^*>\delta t_o^*$).

Kinetic conditions of Dirichlet type are defined on the oil-water interface Σ, where the velocity potential $\phi^*(t^*)$ is known. At the initial moment, the interface is considered slightly upward oriented (as a non-flat meniscus), and the velocity potential is assumed to be $\phi^*(t^*=0)=z^*v_n^*(t^*=0)$. For any further moment, the velocity potential $\phi^*(t^*>0)$ on Σ is obtained within the BEM.

② The time progression, made with an explicit numerical scheme of 4th order Runge-Kutta type [18], allows the connection of two successive steps, to determine the new potential values and interface position at the following instant $(t^*+\Delta t^*)$. The time step Δt^* is selected upon a stability criterion, linked to gravity-capillary dispersion equation [19]:

$$\Delta t^*\le 2\left(\frac{\pi^3}{We\left(\Delta s_{\min}^*\right)^3}+\frac{\pi}{Fr\,\Delta s_{\min}^*}\right)^{-0,5}\ , \qquad (12)$$

where $\Delta s_{\min}^*$ is the minimum length of a boundary element considered on $\Sigma_\Omega(t^*)$. The temporal interface evolution is determined through a Lagrangian description of a variable number of nodes, unevenly redistributed on the boundary $\Sigma_\Omega(t^*)$ at each time step, with respect to the adaptation at surface gradients [16].

In the absence of non-linear analytical tests, the evaluation of numerical code accuracy is checked through the global mechanical energy balance (11). Upon azimuthal integration, the mechanical energy balance deals with line integrals of the terms computed through the BEM, thus being easily implemented in the computational procedure.

4. NUMERICAL RESULTS

Within this paper, the BEM simulations point on the liquid-liquid interface evolution for the case of upwards oil injection through a vertical nozzle submerged in water.

An olive oil – water couple has been selected. The physical properties of those liquids are [1]: densities $\rho_o = 918$ kg/m^3, and $\rho_w = 1000$ kg/m^3; dynamic viscosities $\mu_o = 0{,}099$ Pa·s, and $\mu_w = 0{,}001$ Pa·s; interfacial tension $\sigma = 0{,}02$ N/m, at 20ºC.

For small orifice sizes, e.g. for $R \le 2{,}5$ mm, the oil-water interface shape evolves like the air-liquid interface of an emerging bubble, formed at a submerged orifice. For an oil-water couple and orifice radius $R = 1$ mm, the dimensionless numbers are $We = 1$, $Fr = 24{,}86$ and $Re = 1{,}368$. For an orifice radius $R = 2{,}5$ mm, the Froude and Reynolds numbers are $Fr = 3{,}978$ and $Re = 2{,}164$. Due to the choice of scales, the Weber number takes always the unit value. The viscous and capillary effects are dominant for very small orifices (say $R \le 1$ mm), and the gravity becomes less important. So, the oil-water interface is less distorted, and continues to grow up till the end of the oil injection (for $t^* > \delta t_o^*$), then it detaches after a complete necking of the interface near the orifice. Within this paper, the oil-interface evolution for small orifice sizes is not presented, because it does not correspond to a vortex ring formation.

For large orifice sizes, e.g. for $R \ge 5$ mm, the oil-water interface evolves from a sessile shape, to a cap profile with a roll-up border: at the end of the computed process, the velocity field behaviour leads to an inward rolling up movement of the cap border, simultaneously with the interface necking near the orifice level. Such velocity field precedes typically a vortex ring formation. Further, numerical results are presented for large orifice radius cases.

When increasing the orifice radius, the Froude number decreases drastically, so the effect of the gravity becomes more and more important. Over the whole orifice radius range, the Reynolds number keeps very small values, so the viscous effects always remain important.

The oil-water interface evolution is discussed firstly for an orifice radius $R = 7{,}5$ mm, with the following corresponding dimensionless numbers: $We = 1$, $Fr = 0{,}442$ and $Re = 3{,}748$.

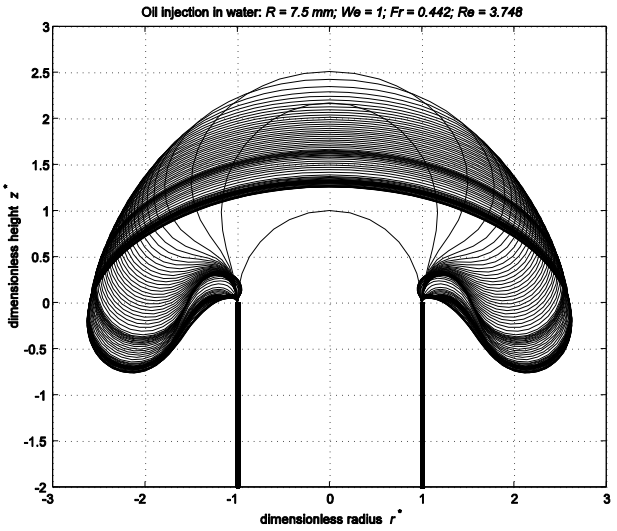

Figure 2. Oil injection in water (superposed frames) $R = 7{,}5$ mm ($We = 1$, $Fr = 0{,}442$ and $Re = 3{,}748$)

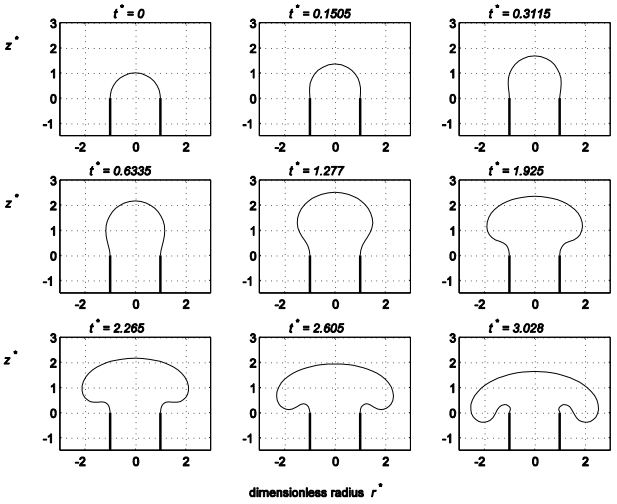

Figure 3. Oil injection in water (separate frames) $R = 7{,}5$ mm ($We = 1$, $Fr = 0{,}442$ and $Re = 3{,}748$)

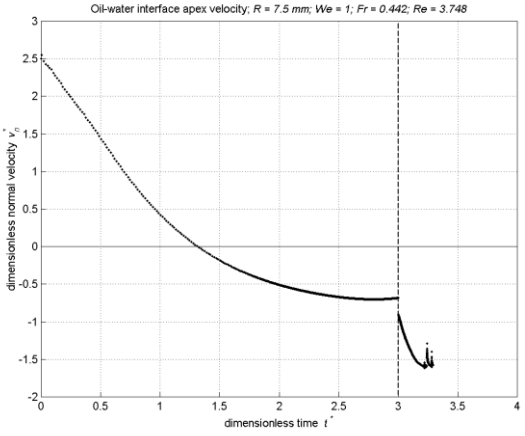

Figure 4. Velocity of the oil-water interface apex versus time, for $R = 7{,}5$ mm

The choice of the value of that radius is due to the classical case presented by Batchelor [1, plate 20], for a vortex ring formed in water by the injection of coloured liquid of almost the same density as water, from an orifice of 7,5 mm-radius.

In Figure 2, we present superposed frames of the interface evolution corresponding to the oil in water injection, when applying a velocity $v_{no}^{*} = 2{,}5$ on Σ_o during a time pulse $\delta t_o^{*} = 3$. The same evolution, in separate frames at different moments $t^{*} \in [0; 3{,}028]$, is presented in Figure 3.

The variation of the velocity of the interface apex (the node placed on the Oz axis) versus time is presented in Figure 4. The moment $t^{*} = \delta t_o^{*} = 3$ is marked on the diagram: before that moment, the apex velocity decreases monotonously; when the oil injection is stopped, there is a drop in apex velocity; then, it continues to oscillate due to inertial effects.

In Figure 5 we present the velocity vectors (with their size and direction) in each node of the interface, at the same time moments as in Figure 3. For $t^{*} > 1{,}9$ the velocity field behaviour leads to an inward rolling up movement of the cap border. For $t^{*} > \delta t_o^{*}$, the roll-up is amplified by the interface necking that starts near the orifice level. This velocity field is supposed to lead to the oil drop detachment and vortex ring formation (the present computations are not preformed till the complete necking and interface rupture).

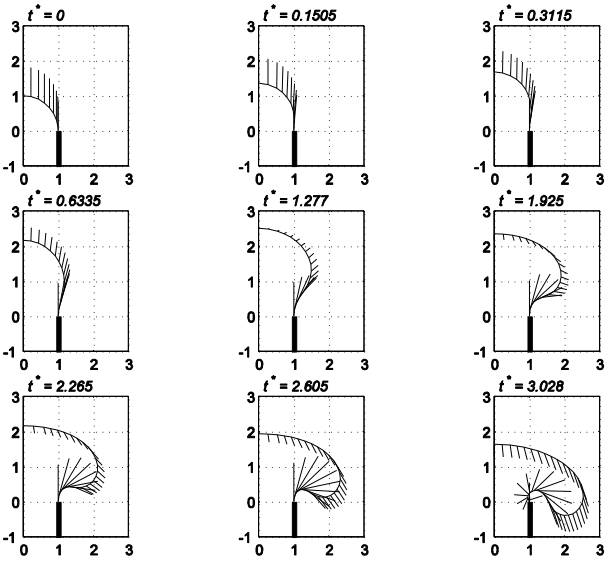

Figure 5. Velocity vectors in each node of the oil-water interface at different moments for $R = 7{,}5$ mm

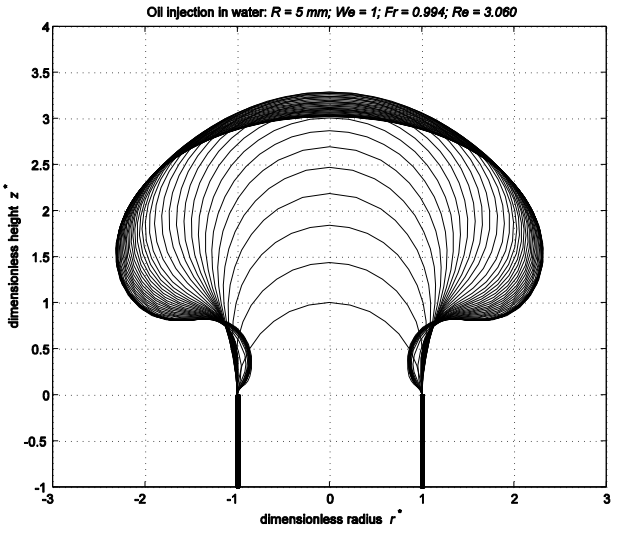

Figure 6. Oil injection in water (superposed frames) for $R = 5$ mm

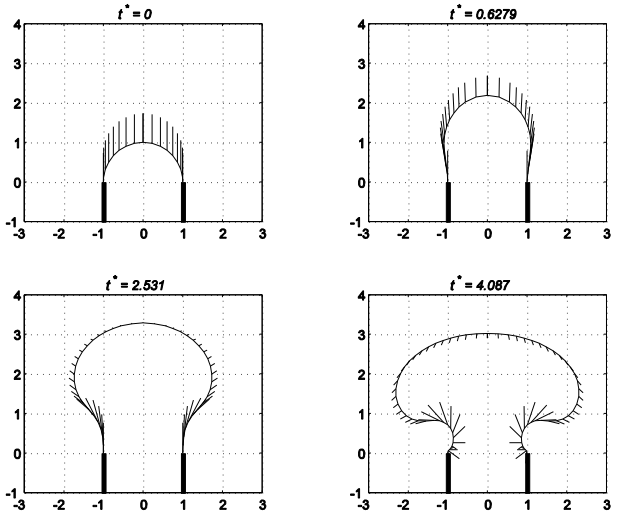

Figure 7. Velocity vectors in each node of the oil-water interface at different moments for $R = 5$ mm

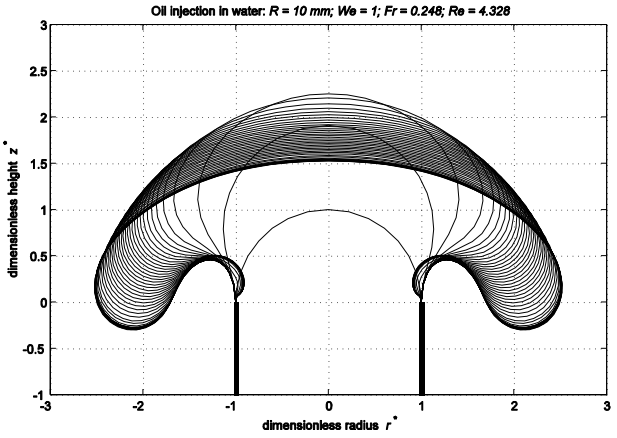

Figure 8. Oil injection in water (superposed frames) for $R = 10$ mm

In Figures 6 and 7, we present superposed frames of the interface evolution, and the velocity vectors in each node of the interface, for the case of an orifice with a radius $R = 5$ mm, the oil being injected with a velocity $v_{no}^* = 2{,}2$ on Σ_o during a time pulse $\delta t_o^* = 4$. The corresponding dimensionless numbers are: $We = 1$, $Fr = 0{,}994$ and $Re = 3{,}060$.

As depicted from the last frame of Figure 7 (at $t^* = 4{,}087$), the velocity field behaviour near the orifice corresponds to a slight rolling up movement of the cap border, with respect to the previous case (see last frame of Figure 5, for $R = 7{,}5$ mm).

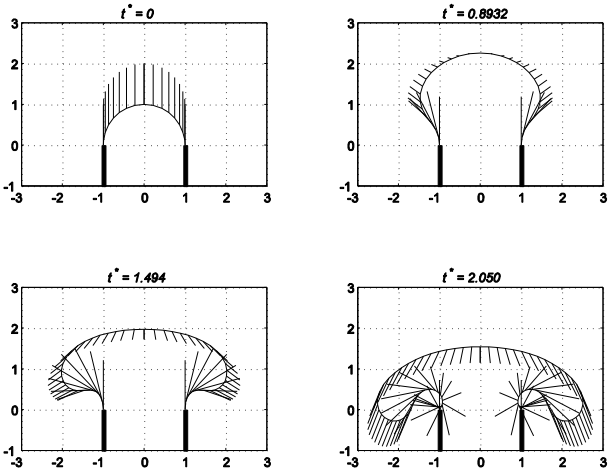

Figure 9. Velocity vectors in each node of the oil-water interface at different moments for $R = 10$ mm

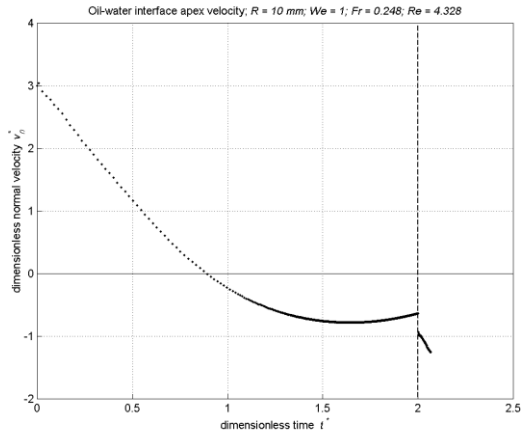

Figure 10. Velocity of the oil-water interface apex versus time, for $R = 10$ mm

In Figures 8 and 9, we present superposed frames of the interface evolution, and the velocity vectors in each node of the interface, for the case of an orifice with a radius $R = 10$ mm, the oil being injected with a normal velocity $v_{no}^* = 3$ on Σ_o during a time pulse $\delta t_o^* = 2$. The corresponding dimensionless numbers are: $We = 1$, $Fr = 0{,}248$ and $Re = 4{,}328$.

As depicted from the last frame of Figure 9 (at $t^* = 2{,}050$), the velocity field behaviour near the orifice corresponds to a stronger rolling up movement of the cap border, with respect to both previous cases (see the last frame of Figure 5, for $R = 7{,}5$ mm, and the last frame of Figure 7, for $R = 5$ mm).

The variation of the velocity of the interface apex upon time, for the orifice with $R = 10$ mm, is presented in Figure 10. The moment $t^* = \delta t_o^* = 2$ is marked on the diagram: the apex velocity decreases before that moment, then, when the oil injection is stopped, there is a drop in apex velocity. After that velocity dropping, the apex velocity continues to decrease, without oscillating like for smaller orifice radius cases. Due to the fact that the gravity force becomes dominant over the capillary and viscous forces for such great orifice radius, after stopping the oil injection, the necking of the interface will continue and the cap border is supposed to continue to roll up simultaneously.

5. CONCLUSIONS

The interface evolution during the oil injection in water has been modelled through BEM, in a viscous potential flow assumption. For large nozzle orifices, the oil-water interface evolves from a sessile shape, to a cap profile with a roll-up border. It is supposed that the process ends by the complete necking of the interface near the orifice, and a vortex ring formation.

First of all, it must be highlighted that we do not dispose of any experimental or numerical evidence on the oil injection in water from a submerged orifice, not even for other liquid-liquid couples characterised by an interfacial tension. Within the existing experimental and theoretical evidence related to a liquid injection into another liquid, there is not a well delimited interface between the two liquids: usually, the injected liquid is the same (coloured or not) as the surrounding-one.

We found that at the end of the computed process, the velocity field behaviour leads to an inward rolling up movement of the interface cap border, simultaneously with the interface necking near the orifice level. Such velocity field precedes typically a vortex ring formation. It is obviously